Journal of Alloys and Compounds 509 (2011) 8748–8755

Contents lists available at ScienceDirect

Journal of Alloys and Compounds

journal homepage: www.elsevier.com/locate/jallcom

Optoelectronic studies of sol–gel derived nanostructured CdO–ZnO composite films

A. Abdolahzadeh Ziabari, F.E. Ghodsi*

Department of Physics, Faculty of Science, The University of Guilan, Namjoo Avenue, P.O. Box 41335-1914, Rasht, Iran

ARTICLE INFO

Article history:
Received 26 April 2011
Received in revised form 8 June 2011
Accepted 13 June 2011
Available online 21 June 2011

PACS:
78.20.Ci
81.20.Fw
73.63.Bd

Keywords:
Optical constants
Sol–gel
CdO–ZnO thin films
Electrical properties

ABSTRACT

Compositional dependence of the optoelectronic properties of sol–gel derived CdO–ZnO composite films with volume ratio of Cd:Zn ranging from 1:0 to 0:1 (with a step of 1/4) has been studied. After heat treatments in air the prepared thin films were investigated by studying their structural, morphological, d.c. electrical and optical properties. X-ray diffraction (XRD) results suggest that the samples are polycrystalline and the crystallinity of them increased with Cd ratio. The average grain size is in the range of 20–34 nm. As composition and structure changed due to the Cd volume ratio, the order of the carrier concentration was varied from 10^{16} to 10^{20} cm^{-3} with Cd ratio and the mobility increased from less than 2 to 45 cm^2 V^{-1} s^{-1}. It was found that the transmittance and the band gap decreased as Cd ratio increased. The optical constants of the film were studied and the dispersion of the refractive index was discussed in terms of the Wemple–DiDomenico single oscillator model. The real and imaginary parts of the dielectric constant of the films were also determined. The volume energy loss (VELF) increases more than the surface energy loss (SELF) at their particular peaks. The third-order nonlinear polarizability parameter is higher for CdO–ZnO thin films with higher concentration of cadmium oxide.

1. Introduction

Transparent conducting oxides (TCOs) have been extensively studied because of their applications in semiconductor optoelectronic device technology. Some of these transparent metallic oxides include, in part, zinc oxide (ZnO), indium–tin oxide (ITO), tin oxide (SnO_2) and cadmium oxide (CdO). CdO and ZnO are both promising materials for their applications as window and buffer layers in thin film solar cells. CdO is an n-type semiconductor, with a direct band gap of approximately 2.5 eV [1] which is lower than that of ZnO (~3.3 eV [2]), however CdO thin films show low resistivity with respect to the high values obtained for ZnO. It is known that it is difficult to obtain simultaneously a high transmission in the visible region and good conductivity qualities [3]; however, a ternary compound which combines these properties in a controlled way may allow the optimization of the window layer on solar cells. Since Zn and Cd belong to the same group in the Periodic table, it is of both fundamental and practical interest to study the Cd–Zn–O ternary system. Cadmium zinc oxide (CdO–ZnO), the ternary TCO material, is a transparent conductor material that combines many beneficial characteristics of both CdO and ZnO. The ratio of Cd and Zn cations becomes important for obtaining a TCO film. Since the first report in 1996 [4], a spate of studies have begun to appear on Cd–Zn–O thin films, nanowires and nanorods [5–14]. These interesting materials have been synthesized by various techniques, including electrodeposition [5], molecular beam epitaxy [6], sol–gel [7–10], thermal decomposition technique [11], pulsed laser deposition [12], spray pyrolysis [13] and ultrasonic spray pyrolysis (USP) technique [14]. The sol–gel process has been widely used for preparing nanostructured films of different materials and devices, which is considered as a facile route for a large-area coating at relatively low temperature and low cost. Sol–gel dip-coating is a thin film deposition technique that has many profits such as easier composition control, better homogeneity and lower cost. The study about the preparation and characterization of sol–gel derived CdO–ZnO thin films is very extensive; however, most of the works have been carried out by using spin-coating technique and the reports about dip-coated CdO–ZnO thin films are scarce [15]. In the present study, a series of CdO–ZnO thin films (with volume ratio of Cd:Zn ranging from 1:0 to 0:1) have been prepared by the sol–gel dip-coating route combined with a heat-treating process.

Despite numerous papers focus on CdO–ZnO thin films, most of them have been concentrated on the preparation of CdO–ZnO alloy films and knowledge of the physical properties of these films is very limited [16]. It is particularly important to study the system of the two materials, as to how the morphology, electrical conductivity, band gap and optical constants are altered when the composition changes. Furthermore, studying the correlations

* Corresponding author.
E-mail address: feghodsi@guilan.ac.ir (F.E. Ghodsi).

0925-8388/$ – see front matter.
doi:10.1016/j.jallcom.2011.06.050

between mentioned properties fundamentally, allows us to understand the phenomenological features of such alloys. Caglar et al. [7] have reported the experimental results about the variation of the structural, morphological, optical and electrical characteristics of sol–gel derived CdZnO films with various compositional ratios. It was found that for CdZnO films, the electrical resistivity and the optical transmission were increased when Zn concentration increased. They have reported 91 Ω cm for the minimum value of electrical resistivity and the photosensitivity of the samples has also been investigated. Ilcan et al. [8] have arranged the same experimental process as Caglar et al. to prepare CdZnO thin films with an emphasis on the optical properties of the films. Li et al. [10] have conducted an investigation into the effects of doping concentration and annealing temperature on the structural, morphological, optical and electrical properties for sol–gel derived ZnO:Cd thin films. They have studied the transport properties of ZnO:Cd thin films with thermal activation and the variable range hopping (VRH) model. Lee et al. [17] studied the effect of chemical composition on the optical properties of ZnO:Cd films deposited by the PLD method. As the deposition temperature decreased, the average transmittance decreased accompanied by a shift of absorption edge to the longer wavelength, which was mainly attributed to the change of Cd/Zn ratio.

More literature survey revealed that the discussion about the fundamental physical behavior of CdO–ZnO thin films is very limited. Therefore, in this paper, in addition to the experimental studies of structural, morphological, electrical and optical properties of the prepared CdO–ZnO thin films and investigation of the possible correlations between them we have especially focused on the compositional behavior of the optical (linear and non-linear) features of them fundamentally. To conduct this, in addition to the common methods to determine the optical constants, we have utilized some models such as Wemple–DiDomenico single oscillator model.

2. Experimental details

The following steps were used for the preparation of the CdO–ZnO films: at first, zinc acetate dihydrate [$Zn(COOCH_3)_2{\cdot}2H_2O$] and cadmium acetate dihydrate [$Cd(COOCH_3)_2{\cdot}2H_2O$] of 0.5 M were prepared separately. 2-Methoxyethanol ($C_3H_8O_2$) and monoethanolamine (C_2H_7NO, MEA) were used as a solvent and stabilizer, respectively. In order to prepare ZnO precursor solution, MEA was dissolved in 2-methoxyethanol initially. Subsequently, zinc acetate dihydrate was added to the solution. The resulting mixture was stirred at room temperature for 1 h to yield a colorless and transparent solution. CdO solution was prepared by the same manner. The obtained solutions were mixed together in different volume ratios. The composite CdO–ZnO thin films were named hereafter S_1, S_2, S_3, S_4, and S_5, corresponding to volume ratio of Cd:Zn of 0:1, 1/4:3/4, 1/2:1/2, 3/4:1/4, and 1:0. Then each of those was stirred constantly for 1 h at room temperature. The final clear solutions were aged for 24 h before the CdO–ZnO thin films dip-coated onto soda lime glass substrates.

Fig. 1 shows a flowchart of the procedure that was used for depositing the CdO–ZnO thin films using sol–gel dip-coating route. Before dip-coating, the glass substrates were first degreased by detergent, rinsed thoroughly by deionized water and then in boiled water. In order to remove macroscopic contaminations, the substrates were cleaned ultrasonically in a mixture of ethanol and acetone (each of 50% in volume) for 15 min. The latter procedure, then repeated in deionized water. At least, the substrates were immerged in acetone and rinsed with deionized water and dried with Nitrogen. The cleaned substrates were dipped into the solution and withdrawn from it vertically at a speed of ~106 mm/min. After the dip coating the film were dried at 275 °C for 10 min in an oven to evaporate the solvent and for gel formation. This procedure was repeated 10 times, and finally the resulting thin films were annealed at 450 °C in air for 1 h.

3. Characterization

The crystalline structure and the texture of the films were carried out by XRD measurements (XRD6000, Shimadzu system with Cu K_α radiation wavelength of 0.15406 nm). Quantitative analyses were obtained by an energy dispersive X-ray analysis (LEO, 1430VP) with accelerating voltage 17 kV. For surface analysis and structure we used the AFM technique. AFM experiment was carried out in the ambient condition using Veeco CP Research instrument using Si cantilever. The optical transmission spectra of the films were measured using a Varian Cary100 UV/Visible spectrophotometer. The electrical measurements were carried out using the Van der Pauw's technique with a RH2010 Van der Pauw and Hall effect measurement system. The optical constants of the films were calculated using pointwise unconstrained minimization approach [18].

4. Results and discussion

4.1. Structural and morphological properties

In Fig. 2 the representative XRD patterns for CdO–ZnO thin films deposited at different Cd volume ratios in solution are presented. XRD studies were carried out in order to get an idea of the structural changes produced in CdO–ZnO films as a result of the increase of Cd content. Comparisons of the related diffractograms (Fig. 2) show variation in both peak position (2θ) and intensity. As a matter of fact, in all the XRD patterns (S_2, S_3 and S_4), peaks of ZnO and CdO are present. The observed diffraction peaks (1 0 0), (0 0 2) and (1 0 1) for ZnO and (1 1 1), (2 0 0) and (2 2 0) for CdO are in good agreement with the reported data [19,20]. By employing the Scherrer's formula, the average grain size was calculated for all samples. It was found that the grain size increases from 20 to 34 nm, when Cd ratio increases. This can be ascribed to the larger ionic radius of Cd^{2+} (0.74 Å) than that of Zn^{2+} (0.60 Å). The quantitative analysis of the nanocrystals was carried out by using energy dispersive X-ray (EDX) analysis to study stoichiometry of nanostructured thin films. The results exhibit (not shown here) the presence of Cd and Zn picks with Cd/Zn atomic percentage ratio of 0.17, 0.44 and 1.55 for S_2, S_3 and S_4, respectively. The corresponding nominal solution values are 0.40, 1.20 and 3.60, respectively. It can be seen that film composition is always lower in Cd than the corresponding nominal solution values. Based on Clausius–Clapeyron equation, the vapor pressure of Cd at 450 °C is about 13 times higher than the vapor pressure of Zn. Therefore, it is possible to conclude that re-evaporation of Cd from substrate at a higher rate than Zn explains why the ratio of atoms of Cd/Zn in the film final composition is lower than nominal value. Microroughness of thin films plays a vital role for developing optical coatings especially in the UV region [21] for applications such as lithographic uses [22].

Surface morphology of the present CdO–ZnO films is shown in Fig. 3. The 1 μm × 1 μm AFM images are utilized for measuring the surface roughness of the films. The root mean square (RMS) roughness of the films varies from 1.52 to 4.08 nm with increasing Cd concentration. It is also evident that, the particles size increases with increasing Cd content. It is probably due to the better crystallinity formed after increasing the Cd ratio. The roughness of the sample not only describes the light scattering but also gives an idea about the quality of the surface under investigation. Khan et al. [23] have reported a kind of inverse trend of resistivity with roughness of nanostructered SnO_2 thin films. In fact, we have observed a similar behavior in the present sol–gel derived CdO–ZnO thin films. With roughness, the resistivity of the samples decreased from 3.3×10^2 to 34×10^{-3} (Ω cm). The increase in surface roughness upon increasing Cd concentration is the concomitant result of grain size increasing. It is commonly recognized that the resistivity will be enhanced with roughness increasing. Though the contributions to ρ are from many sources, due to polycrystalline nature of the present films, grain boundary scattering is present at all the samples. From XRD results, it is noted that the grain size increases with Cd content. When the number of grains are decreased (or the grain size increased) the grain boundary scattering gets reduced and hence resistivity of the film. This is reflected in resistivity and

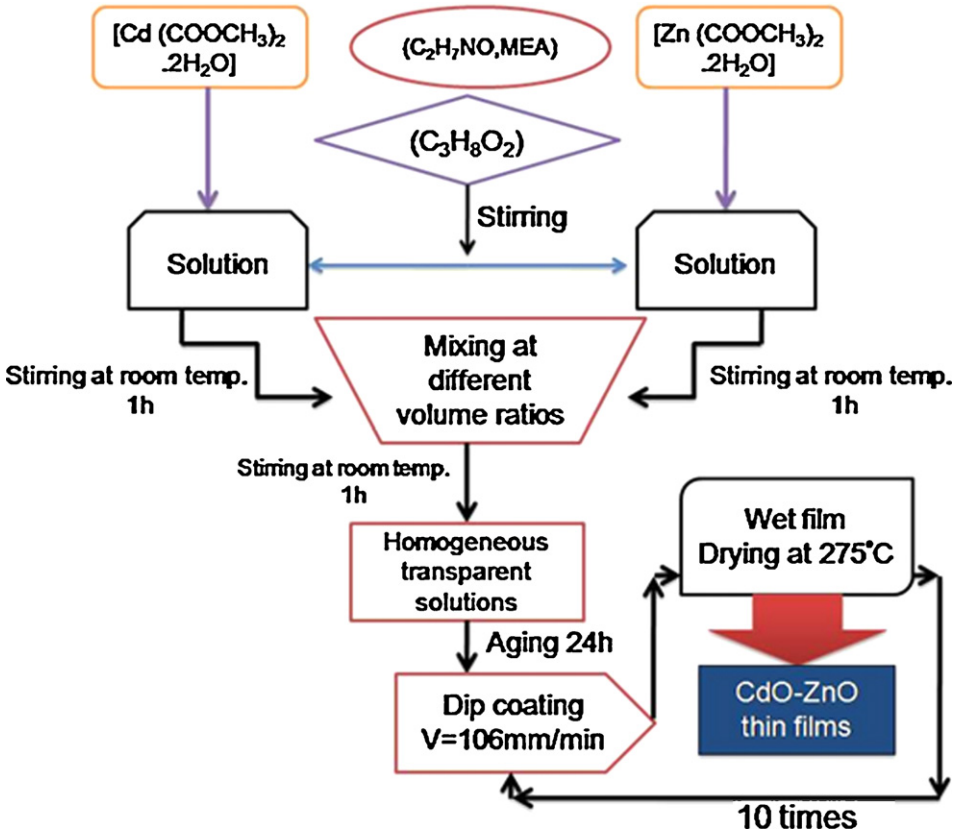

Fig. 1. The flowchart of the procedure of preparing CdO–ZnO thin film.

can be seen in Fig. 4. In the case of S_5, according to XRD result the grain size is larger than S_1 and its surface roughness is also high as per AFM studies. Therefore, in this film, the contribution from grain boundary scattering to the resistivity can be expected to be minimum.

4.2. Electrical properties

The behavior of carrier concentration (n), resistivity (ρ) and carrier mobility (μ) is shown in Fig. 4. Film thickness was about 140 nm for all the films. It is evident that the carrier concentration increases with Cd ratio up to Cd1/2:Zn1/2 (sudden increase in Cd1/2:Zn1/2) and after that decreases slightly with further increase in Cd ratio. The conduction electrons in undoped metal oxide thin films are supplied from donor sites associated with oxygen vacancies and the

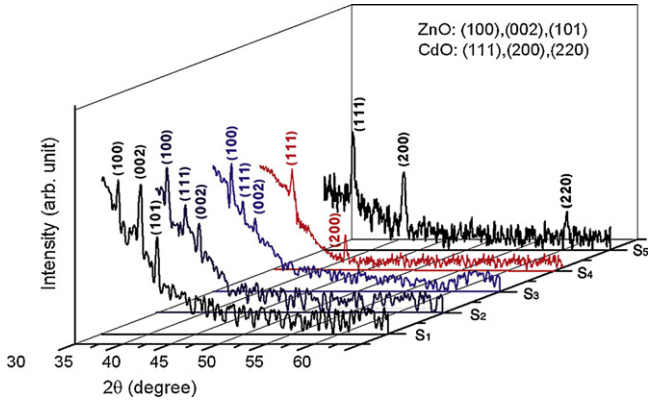

Fig. 2. XRD patterns of CdO–ZnO thin films with different Cd:Zn ratios: S_1 (0:1), S_2 (1/4:3/4), S_3 (1/2:1/2), S_4 (3/4:1/4) and S_5 (1:0).

corresponding metal interstitials. Each oxygen vacancy contributes two electrons to the conduction band, thereby increasing the carrier concentration. It should be noted that an oxygen vacancy in the ZnO lattice usually acts as a donor that generates a single electron [24]. So it is why as the Cd content increases the carrier concentration increases. Since electrons in the CdO–ZnO films are supplied from oxygen vacancy in the film, the decrease of free carrier concentration after Cd1/2:Zn1/2 may be due to decrease of oxygen vacancies, resulting in slight increase of resistivity. The decrease of oxygen vacancies for higher Cd doping may be linked to the fact that low and almost no deviation from stoichiometry exists for high cadmium doped ZnO and undoped CdO films (i.e. S_4 and S_5, respectively) elaborated by sol–gel technique. The carrier mobility increases from 1.5 to 45 $cm^2\,V^{-1}\,s^{-1}$ for S_1–S_5, respectively.

The mobility of charge carriers depends on the scattering mechanisms. It is well known that the acoustical scattering, ionized impurity scattering, and grain boundary (GB) scattering determine the mobility of the charge carriers in TCOs. The acoustical scattering is dominant only in high temperatures. In polycrystalline materials, it is often presumed that grain boundaries scatter charge carriers causing a reduction in mobility relative to single crystals. It is well established that grain boundaries contain fairly high densities of interface states which trap free carriers from the bulk of the grains. It usually assumed that the major contribution to the density of these states comes from the excess oxygen that accumulates at the grain boundary depletes part of the grain of free carriers.

Fig. 5 shows a polycrystalline material composed of grains joined together through grain boundaries. For simplicity, the grain is assumed to be a square having a grain size of D (the larger grain size the narrower grain boundary). At the grain boundaries a back-to-back Schottky barrier is formed. Therefore such a grain boundary may be thought of as a potential barrier for electrons characterized by its width δ and height ϕ_b. The carrier trap density

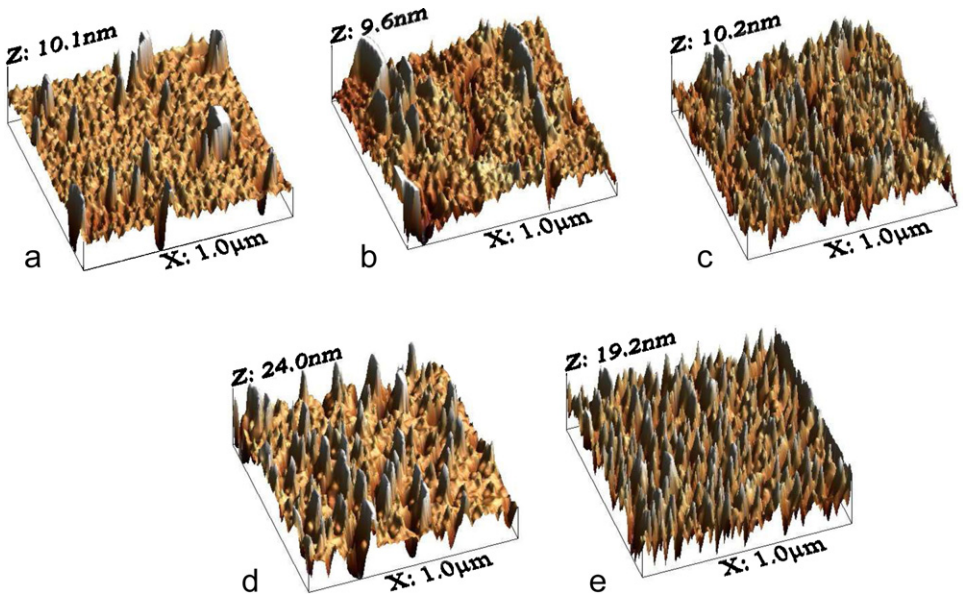

Fig. 3. AFM images (1 μm × 1 μm) showing the surface morphology of CdO–ZnO thin films with different Cd:Zn ratios (a) S_1 (0:1), (b) S_2 (1/4:3/4), (c) S_3 (1/2:1/2), (d) S_4 (3/4:1/4) and (e) S_5 (1:0).

is represented by $Q_t = N\delta$, where N is the donor concentration in the bulk region. The extension of the depletion layer in the bulk of the grain is divided into two cases, depending on whether (a) $Q_t > ND$ or (b) $Q_t < ND$ (where D is the grain size) [25]. For the two situations above we get different dependence on the donor concentrations; in the case (a), the potential barrier increases linearly with the donor concentration: $\phi_b = q^2D^2N/8\varepsilon$, where ε is the static dielectric constant. In the case (b) where we have high donor concentration the grain boundary barrier is inversely proportional N which means it decreases for higher doping: $\phi_b = q^2Q_t^2/8\varepsilon N$. In the latter case, only part of grain is depleted of carriers and the carrier concentration in the bulk region n is almost equal to the donor concentration N.

According to the mentioned relations for ϕ_b, as S_3, S_4 and S_5 films have a higher carrier concentration and a large grain size, the barrier height must be decreased drastically in comparison with S_1 and S_2 and the depletion layer width must be much smaller than the grain size, i.e. $\delta \ll D$ as is in case (b). On the other hand the Fermi level energy in high degenerate samples ($n \geq 3.7 \times 10^{18}$ cm^{-3} [26], i.e. S_3, S_4 and S_5 in the present study) is a function of $n^{2/3}$. So, it can be easily concluded that the degeneracy of the material (i.e. the energy separation between the Fermi level and the conduction band minimum) increases by Cd ratio, an opposite trend respect to ϕ_b. As a result, for charge carrier concentration above about 10^{20} cm^{-3} the grain barriers are narrow enough so that the high energy electrons are able to tunnel through the barriers. On the other hand, scattering by grain boundaries can be remarkable in the case of nondegeneracy with lower carrier concentration (i.e. S_1 and S_2 films in the present study).

4.3. Optical properties

The optical properties of CdO–ZnO thin films were also studied. Fig. 6 shows the transmittance spectra of the prepared films for different concentration of Cd percent in the wavelength range from 250 to 800 nm. It is evident that the transmittance decreases with Cd content to reach its minimum value at Cd1:Zn0 (i.e. S_5 sample). This behavior can be attributed to the higher value of the surface roughness of the films with higher Cd content due to the increased optical scattering of incident light on the film surface [27].

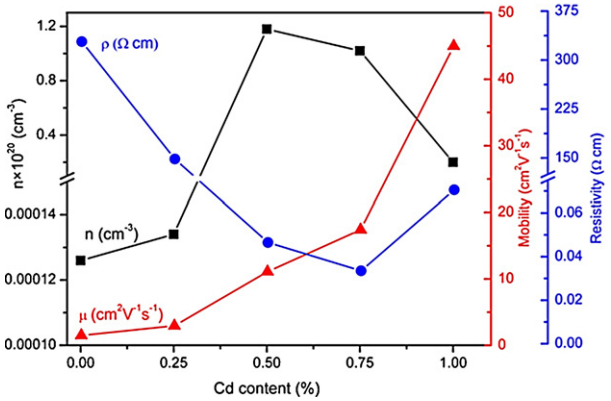

Fig. 4. Plots of carrier concentration (n ■), carrier mobility (μ ▲) and resistivity (ρ ●) as a function of Cd content for CdO–ZnO thin films.

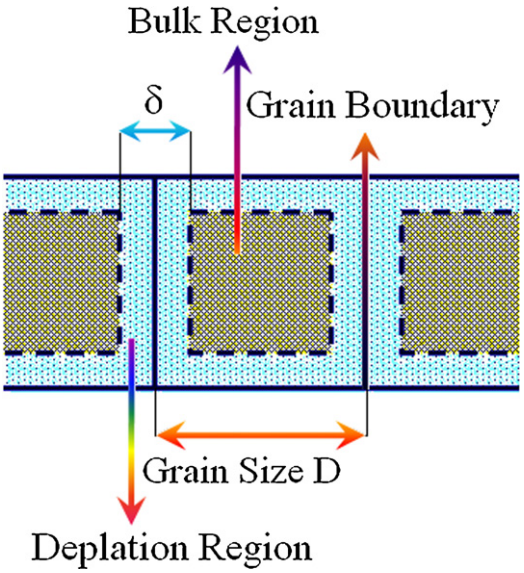

Fig. 5. Model for the crystal structure of polycrystalline films [15].

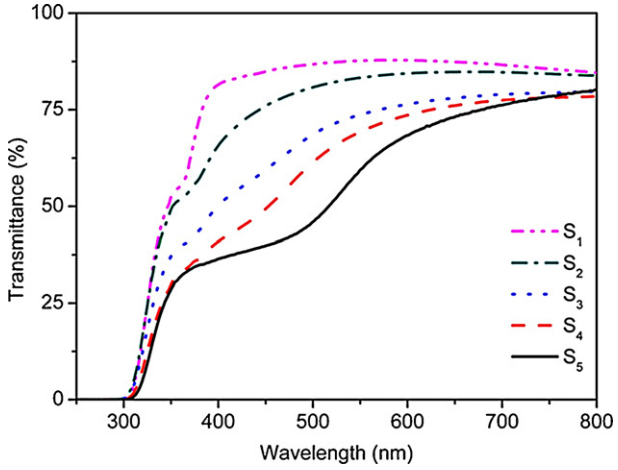

Fig. 6. Transmittance spectra of CdO–ZnO thin films with various Cd content.

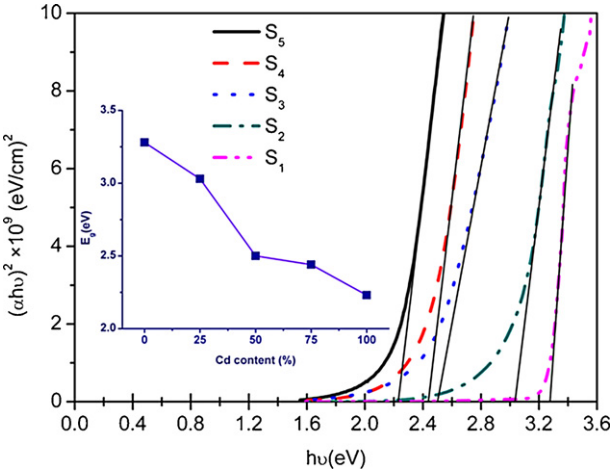

Fig. 7. Determination of the optical band gaps from the plots of $(\alpha h\nu)^2$ vs. photon energy, $h\nu$, for composite CdO–ZnO film with different Cd:Zn ratios: S_1 (0:1), S_2 (1/4:3/4), S_3 (1/2:1/2), S_4 (3/4:1/4) and S_5 (1:0).

The optical absorption coefficient α was evaluated from the optical transmission data in the region of strong absorption using [28]

$$\alpha = \frac{1}{d} Ln\left(\frac{(n+1)^3(n+s^2)T}{16n^2 s}\right) \quad (1)$$

where d, n and s are the thickness, the refractive index of the film and the refractive index of the substrate, respectively. The dependence of α with the photon energy $h\upsilon$ is fitted to the relationship for the allowed direct transition

$$\alpha h\nu = A(h\nu - E_g)^{1/2} \quad (2)$$

where A is the band edge constant. The optical band gap E_g values were obtained by extrapolating the linear portion of the plots of $(\alpha h\upsilon)^2$ vs. $h\upsilon$ to $\alpha = 0$ (Fig. 7). The corresponding E_g values are given in Table 1. Apparently, as the optical band gap decreases from 3.28 eV to 2.23 eV (shown in the inset of Fig. 7); the optical absorption edge exhibits a redshift with the rise of Cd concentration from 0 to 100%. The narrowing band gap is due to the existence of Cd impurities in the ZnO structure, which induce the formation of new recombination centers with lower emission energy [9]. Zhang et al. [29] performed a first-principles study and employed the Perdew–Burke–Ernzerhof form of the generalized gradient approximation to evaluate the electronic and optical properties of ZnO:Cd. They obtained that with increasing Cd concentrations, the band gap of ZnO:Cd was decreased due to the increase of s states in the conduction band. Tang et al. [30] applied first-principles calculation with the PAW–GGA method to study wurtzite $Zn_{1-x}Cd_xO$ alloys. They attributed the reduction of band gap with the increase of Cd content to the contributions of the hybridization of electronic states of Zn-4s and Cd-5s, the enhancement of p–d repulsion and the tensile strain due to Cd-doping. The optical constants (n,k) of the films were obtained using pointwise unconstrained minimization algorithm. The influence of the compositional ratio of Cd on the refractive index and the extinction coefficient of the films are presented in Figs. 8 and 9. The refractive index of all samples is fairly constant in long wavelengths and thoroughly changed from 1.7 to 2.5 with Cd content. It can be distinguished from Fig. 8 also that n values increase with photon energy (in short wavelengths) and the refractive index values of the films show significant differences. This is due to the major contribution of virtual electronic transitions in the thin films. This leads to a significant change in the optical parameters.

The source n (dispersion) is carriers (electron/hole) or phonon of a material. Electromagnetic waves with (long) short wavelengths are dispersed by (phonon) electron. The extinction coefficient of the films also varies as the same manner as the refractive index. The source k (absorption) refers to the inelastic scattering of the electromagnetic waves in the semiconductor such as the Compton effect, photoelectric effect, pair production effect and so on [31]. Totally, the refractive index and the extinction coefficient of the films have an inverse relation with the transmittance spectrum. The (low) high transmittance spectra have (high) low optical constants. Meanwhile, the refractive index decreases with increasing wavelength. This suggests that the CdO–ZnO thin film shows a normal dispersion. Thus, we can analyze the dispersion data of the refractive index by a single-oscillator model [32]

$$n^2 = 1 + \frac{E_d E_o}{E_o^2 - (h\nu)^2} \quad (3)$$

where E_o is the average excitation energy for electronic transitions and E_d is the dispersion energy which is a measure of the strength of interband optical transitions. This model describes the dielectric response for transitions below the optical gap.

Experimental verification of Eq. (3) can be obtained by plotting $(n^2-1)^{-1}$ vs. $(h\upsilon)^2$. The resulting straight line then yields values of the parameters E_o and E_d, as shown in Fig. 10. At short wavelengths (high energies), a negative curvature deviation is sometimes observed due to the proximity of the band edge or excitonic absorption [32]. As it is clear from Fig. 10 such deviations are obvious in the samples of S_1, S_2 and S_3.

The obtained E_o and E_d values are given in Table 1. The oscillation energy E_o, can be correlated with the optical gap by the empiri-

Table 1
The optical band gap E_g and single-oscillator parameters of CdO–ZnO thin films.

Sample	E_g (eV)	E_o (eV)	E_d (eV)	E_o/E_g	M_{-1} (eV)$^{-2}$	M_{-3} (eV)$^{-2}\times10^{-3}$
S_1	3.28	6.62	11.44	2.01	1.72	39
S_2	3.03	6.24	12.36	2.05	1.98	50
S_3	2.50	5.26	10.96	2.10	2.08	75
S_4	2.44	5.01	13.46	2.05	2.68	107
S_5	2.23	4.50	12.51	2.02	2.78	137

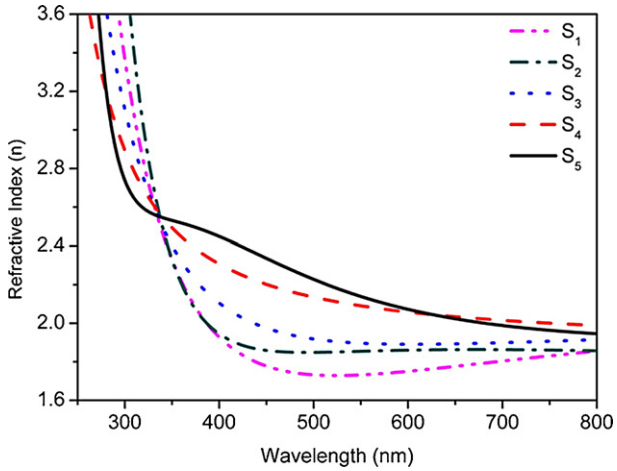

Fig. 8. The dependence of the refractive index of the CdO–ZnO films on the wavelength.

cal formula $E_o \approx 2E_g$. A measure of interband transition strengths can be provided from the M_{-1} and M_{-3} moments of the optical spectrum. The M_{-1} and M_{-3} moments are expressed as [32]

$$M_{-1} = \frac{E_d}{E_o}, \quad M_{-3} = \frac{E_d}{E_0^3} \tag{4}$$

The M_{-1} and M_{-3} moment values are given in Table 1.

It is well-known that polarizabiltiy of any solid is proportional to its dielectric constant. The real and imaginary parts of the complex dielectric constant are expressed as [33]

$$\varepsilon_1 = n^2 - k^2 \quad \text{and} \quad \varepsilon_2 = 2nk \tag{5}$$

where ε_1 and ε_2 are the real and imaginary parts of the dielectric constant, respectively. The variation of ε_1 and ε_2 values of the CdO–ZnO thin films with photon energy at different values of Cd content is shown in Figs. 11 and 12. The real and imaginary parts of dielectric constants follow the same trend but the values of real part are higher than imaginary part. The ε_1 and ε_2 values increase with Cd content. The variation of the dielectric constant with photon energy indicates that some interactions between photons and electrons in the films are produced in this energy range.

Quantities of interest in studying the rate of energy loss for electrons passing through a material are the imaginary part of the reciprocal of the dielectric constant, which is known as the volume energy loss (VELF) and the surface energy loss (SELF) functions. They are related to the real and imaginary parts of the dielectric constant by the following relations [34]

$$\text{VELF} = Im\left(\frac{1}{\varepsilon^*}\right) = \frac{\varepsilon_2}{\varepsilon_1^2 + \varepsilon_2^2} \tag{6}$$

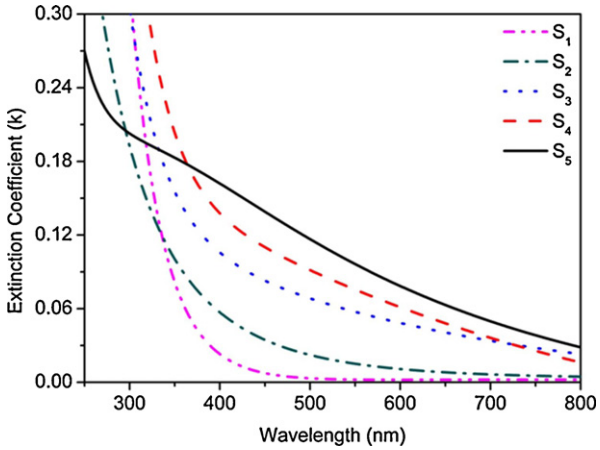

Fig. 9. The dependence of the extinction coefficient of the CdO–ZnO films on the wavelength.

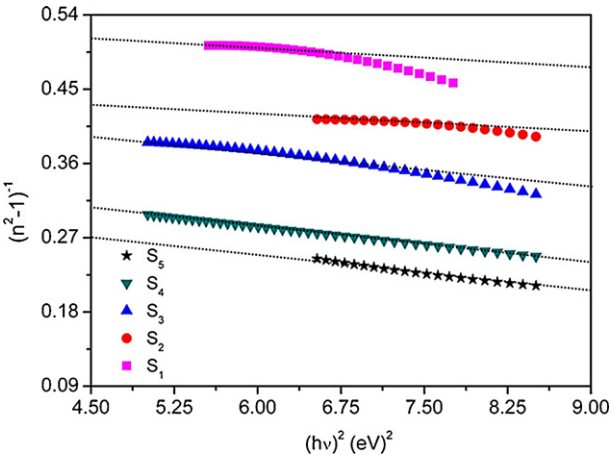

Fig. 10. The $(n^2 - 1)^{-1}$ vs. $(h\upsilon)^2$ plots of the CdO–ZnO thin films.

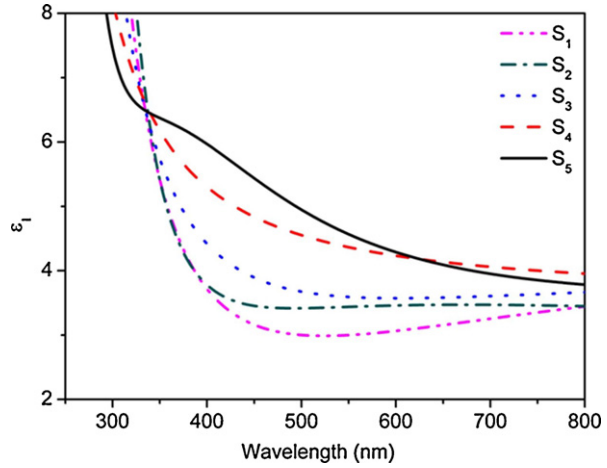

Fig. 11. The variation of real part of the dielectric constant with energy.

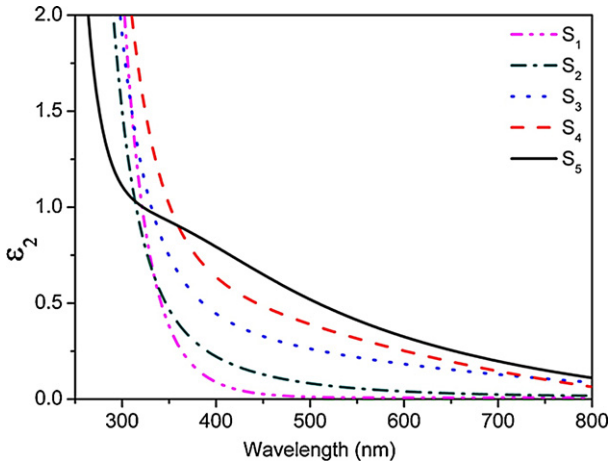

Fig. 12. The variation of imaginary part of the dielectric constant with energy.

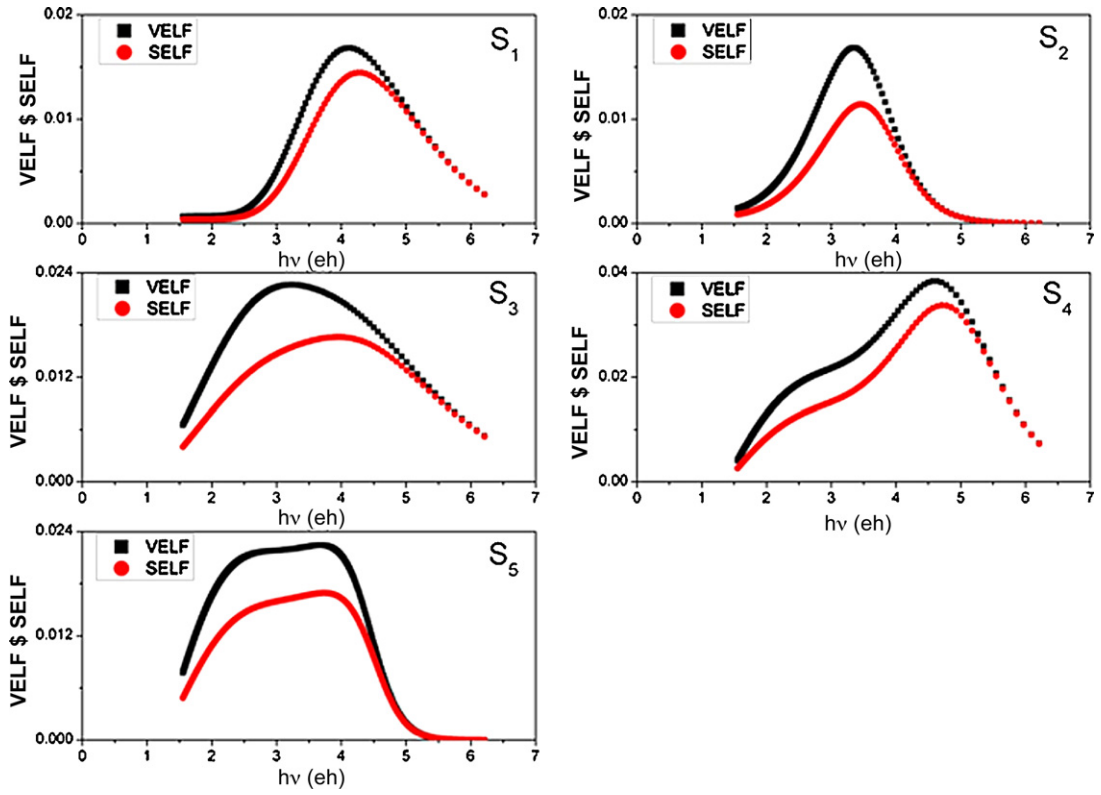

Fig. 13. . Plots of VELF and SELF vs. $h\upsilon$ for composite CdO–ZnO film with different Cd:Zn ratios: S_1 (0:1), S_2 (1/4:3/4), S_3 (1/2:1/2), S_4 (3/4:1/4) and S_5 (1:0).

$$\text{SELF} = -Im\left(\frac{1}{\varepsilon^* + 1}\right) = \frac{\varepsilon_2}{(\varepsilon_1 + 1)^2 + \varepsilon_2^2} \tag{7}$$

These quantities were calculated using real and imaginary parts of the dielectric constant. From the obtained results (Fig. 13), it is clear that the energy loss by the free charge carriers when traversing through the bulk material has approximately the same behavior as when they traverse the surface. It is also clear that there is no significant difference between them at lower and higher photon energies but the VELF increases more than SELF at the particular peak which characterized the CdO–ZnO thin films.

The third-order nonlinear polarizability parameter, $\chi^{(3)}$, so-called nonlinear optical susceptibility, is an important parameter, because it gives an indication about the possibility of using the nanostructured thin films in optical switching. According to Frumer and coworkers [35], the Miller rule is very convenient for visible, nonlinear and near infrared frequencies, which relates the third order of nonlinear polarizability parameter and the linear optical susceptibility, $\chi^{(1)}$, through the equation:

$$\chi^{(3)} = A(\chi^{(1)})^4 = A\left[\frac{E_o E_d}{4\pi(E_o^2 - (h\upsilon)^2)}\right]^4 \tag{8}$$

where $A = 1.7 \times 10^{-10}$ (for $\chi^{(3)}$ in esu). The covalency and ionicity of chemical bonds influence strongly the magnitude of non-linearity. The nonlinear optical susceptibility ($\chi^{(3)}$) of the films as a function of photon energy ($h\upsilon$) has been illustrated in Fig. 14. One can observe that $\chi^{(3)}$ is higher for thin films with higher concentration of cadmium oxide. This means that Cd enriched films at higher ratios of CdO are more suitable for applying as optical switch.

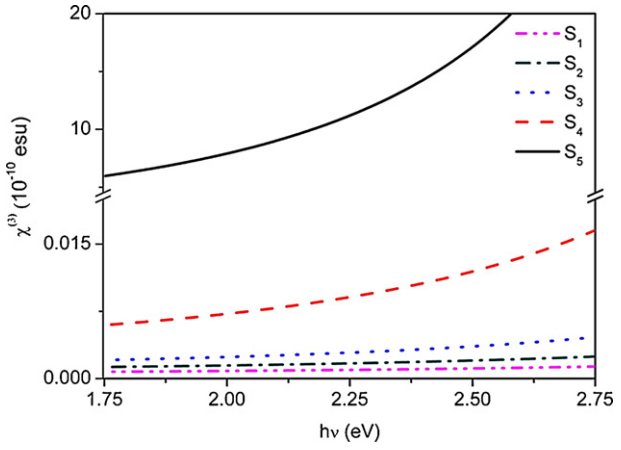

Fig. 14. The nonlinear optical susceptibility $\chi^{(3)}$ as a function of photon energy $h\upsilon$.

5. Conclusion

The structural, morphological, electrical and optical properties of the sol–gel derived CdO–ZnO nanostructured thin films prepared at different Cd content have been investigated. The grain size and surface roughness of the films were increased with Cd content. The carrier concentration and carrier mobility of the samples were increased with Cd ratio whereas in the same time, the resistivity of the films was decreased. The direct optical band gap shifted to the lower energy as a consequence of the increasing of Cd content in the film. Both the refractive index and extinction coefficient are determined. It has been found that the refractive index and extinction coefficient increase with the increasing of Cd content over the entire spectral range studied. The single-oscillator parameter values obtained from Wemple–Didomenico model are correlated with the optical band gap values determined from the Tauc model by an empirical relation: $E_o \approx 2E_g$. Dielectric constant ε was also studied. The real and imaginary part of dielectric constant was increased due to the increase of cadmium oxide

concentration. The third-order nonlinear polarizability parameter $\chi^{(3)}$ of CdO–ZnO thin films has been determined using Miller rule based on Wemple–DiDomenico single oscillator parameters. With the increase in Cd content nonlinear optical susceptibility $\chi^{(3)}$ increases.

References

[1] B. saha, R. Thapa, K.K. Chattopadhyay, Solid State Commun. 145 (2008) 33.
[2] H. Guo, J. Zhou, Z. Lin, Electrochem. Commun. 10 (2008) 146.
[3] K.L. Chopra, S. Major, D.K. Pandya, Thin Solid Films 102 (1983) 1.
[4] Y.S. Choi, C.G. Lee, S.M. Cho, Thin Solid Films 289 (1996) 153.
[5] M. Tortosa, M. Mollar, B. Man, J. Cryst. Growth 305 (2007) 97.
[6] L. Li, Z. Yang, Z. Zuo, J.H. Lim, J.L. Liu, Appl. Surf. Sci. 256 (2010) 4734.
[7] Y. Caglar, M. caglar, S. Ilican, A. Ates, J. Phys. D: Appl. Phys. 42 (2009) 065421.
[8] S. Ilican, Y. Caglar, M. Caglar, M. Kundakci, A. Ates, Int. J. Hydrogen Energy 34 (2009) 5201.
[9] F. Yakuphanoglu, S. Ilican, M. Caglar, Y. Caglar, Superlattices Microstruct. 47 (2010) 732.
[10] G. Li, X. Zhu, X. Tang, W. Song, Z. Yang, J. Dai, Y. Sun, X. Pan, S. Dai, J. Alloys Compd. 509 (2011) 4816–4823.
[11] W.E. Mahmoud, A.A. Al-Ghamdi, Opt. Laser Technol. 42 (2010) 1134–1138.
[12] R. Vinodkumar, K.J. Lethy, P.R. Arunkumar, R.R. Krishnan, N. Venugopalan Pillai, V.P. Mahadevan Pillai, R. Philip, Mater. Chem. Phys. 121 (2010) 406–413.
[13] H. Tabet-Derraz, N. Benramdane, D. Nacer, A. Bouzidi, M. Medles, Sol. Energ. Mater. Sol. Cells 73 (2002) 249.
[14] N. Kavasoglu, A.S. Kavasoglu, S. Oktik, J. Phys. Chem. Solids 70 (2009) 521–526.
[15] G. Torress-Delgado, C. Zúñiga-Romero, O. Jimenez-Sandoval, R. Castanedo-Perez, B. Chao, S. Jimenez-Sandoval, Adv. Funct. Mater. 12 (2002) 129.
[16] S. Vijayalakshmi, S. Venkataraj, R. Jayavel, J. Phys. D: Appl. Phys. 41 (2008) 245403.
[17] S.Y. Lee, Y. Li, J.S. Lee, J.K. Lee, M. Nastasi, S.A. Crooker, A.X. Jia, H.S. Kang, J.S. Kang, Appl. Phys. Lett. 85 (2004) 2.
[18] E.G. Birgin, I. Chambouleyron, J.M. Martínez, J. Comput. Phys. 151 (1999) 862.
[19] M. Ghosh, C.N.R. Rao, Chem. Phys. Lett. 393 (2004) 493.
[20] W.Q. Peng, G.W. Cong, S.C. Qu, Z.G. Wang, Nanotechnology 16 (2005) 1469.
[21] A. Duparre, Handbook of Optical Properties, vol. 1, CRC Press, 1995.
[22] M. Senthilkumar, N.K. Sahoo, S. Thakur, R.B. Tokas, Appl. Surf. Sci. 245 (2005) 114.
[23] A.F. Khan, M. Mehmood, A.M. Rana, M.T. Bhatti, Appl. Surf. Sci. 255 (2009) 8562.
[24] T. Minami, Semicond. Sci. Technol. 20 (2005) 35.
[25] J.W. Orton, M.J. Powell, Rep. Prog. Phys. 43 (1980) 1263.
[26] K. ellmer, J. Phys. D: Appl. Phys. 34 (2001) 3097.
[27] D.C. Paine, T. Whitson, C.O. Yang, J. Appl. Phys. 85 (1999) 8445.
[28] R. Swanepoel, J. Phys. E: Sci. Instrum. 16 (1983) 1214.
[29] X.D. Zhang, M.L. Guo, W.X. Li, C.L. Liu, J. Appl. Phys. 103 (2008) 063721.
[30] X. Tang, H.F. Lu, J.J. Zhao, Q.Y. Zhang, J. Phys. Chem. Solids 71 (2010) 336.
[31] Horst Czichos, Tetsuya Saito, Leslie Smith, Handbook of Materials Measurement Methods, vol. 978, Springer, Leipzig, 2006.
[32] M. DiDomenico, S.H. Wemple, Phys. Rev. B 3 (1971) 1338.
[33] A.K. Wolaton, T.S. Moss, Proc. R. Soc. 81 (1963) 5091.
[34] M.M. El-Nahass, Z. El-Gohary, H.S. Soliman, Opt. Laser Technol. 35 (2003) 523.
[35] T. Wagner, M. Krbal, T. Kohoutek, V. Peina, Mir. Vlek, Mil. Vlek, M. Frumar, J. Non-Cryst. Solids 326–327 (2003) 233.